Journal of Global Environment Engineering, Vol. 7 , pp. 101 - 117, 2001

NUMERICAL ANALYSIS OF HEAT ISLAND PHENOMENA FOR THE CONTROL OF COOLING ENERGY IN CITIES

Yasunobu Ashie[1]
Vu Thanh Ca[2]
Takashi Asaeda[3]

Abstract

Reducing urban heat island was one of the measures indicated in the board outline for the promotion of ameliorating global warming proposed by the Japanese government. To further understand this in more detail, a numerical model coupling the simulations of urban climate and a building air conditioning system was developed. The model was applied to the study of the urban heat island problem in Japan on two scales: a regional scale (480km × 480km) and a local urban scale (500m×500m). In the study on the regional scale, the thermal characteristics of the Kanto region were analyzed and numerical results were compared with measured data. In the study on the local urban scale, a district in the Tokyo Metropolitan Area was quantitatively analyzed, with the results showing that the distributions of ground surface temperature and air temperature were highly affected by land-use and energy consumption.

KEYWORDS: *urban heat island, urban canopy, energy for cooling, COP, air conditioner*

1. Introduction

Reducing urban heat island was one of measures indicated in *the board outline for the promotion of ameliorating global warming* proposed by the Japanese government (Head office of Japanese government for the promotion of ameliorating global warming, 1997). It is evaluated that for every 1℃ increase in the summertime air temperature, the amount of electricity consumption throughout Japan may rise by 600,000 to 1.2 million kW (Japan Electric Association, 1991). This figure, which represents up to 1% of total peak demand for the entire country (Japan Electric Association, 1991), is the equivalent of the output of one medium-size nuclear reactor, or equal to an economic loss of 20 billion yen per year (Mitsubishi Research Institute, 2000). According to data from the District Meteorological Observatory, the average summer temperature in Tokyo has risen by 1.7℃ over the past 100 years (Ashie, 2000). Thus, it can be evaluated that this rise in urban temperature represents a passive economic loss of 3 billion yen in the metropolitan area (Mitsubishi Research Institute, 2000).

1 Dr. Eng., Chief Researcher, Building Research Institute, JAPAN.
2 Ph.D, Department of Civil and Environmental Enginerring, Saitama university, JAPAN.
3 Dr. Eng., Prof., Guraduate School of Science and Engineering, Saitama university, JAPAN.

Together with rough and macro estimations such as these statistics, there are also predictive methods to obtain spatial distributions considering the physical characteristics (e.g. in the Kanto plain: Murakami *et al.*, 1997; Kimura and Arakawa, 1983; Ichinose *et al.*, 1999). However, in almost all of these studies, the anthropogenic heat discharge in the urban areas was given at each computational mesh. Thus, their model cannot be employed for the estimation of cooling energy consumption due to urban heat island.

This study aims at the formulation of a numerical model for the investigation of the thermal structure of the heat island phenomenon and energy load of buildings. The numerical model, named the Urban Climate Simulation System (**UCSS**), is composed of a model for the building air conditioning system and a model for the prediction of the air temperature, wind velocity, humidity and radiation conditions in the urban atmosphere. Also, a dynamical relationship between the urban climate and anthropogenic heat discharge is established. With this model, the cooling energy that could be saved due to a decrease in the heat island intensity can be evaluated. The k-ε model is widely used in the fields of architecture and civil engineering (Murakami *et al.*, 1996; Kitada *et al.*, 1998). To improve the accuracy of the standard k-ε model, several improvements were incorporated into the model. The thermal diffusion and eddy viscosity were modified by the IP theory (Launder, 1975) which is equivalent to the well-known Level 2.5 of Yamada (1975), as well as the effect of buildings on the turbulence in and outside the urban canopy layer. The model was used for the prediction of the urban heat island and the characteristics of cooling energy consumption at two scales (regional and local) in the center of Japan.

2. Turbulence modeling of urban boundary layer

1) Calculation of the drag effect of building

Strictly speaking, it is necessary to establish detailed boundary conditions for building shape. However, in meso-scale analysis, it is not possible to simulate the flow around each building. Thus, a special spatial averaging procedure was applied to the Navier-Stokes equations and equations for heat and moisture transfer. Effective volume ratio G is defined in the next equation.

$$G = \frac{V_a}{V_o} \qquad (1)$$

Here Va is the air volume of the mesh, V_0 the volume of the mesh including air and solid. Eq. (2) suggests the theory on spatial averaging of function f (Craspite *et al.*, 1986).

$$\left\langle \frac{\partial \overline{f}}{\partial x_i} \right\rangle = \frac{1}{G} \frac{\partial \left\langle \overline{f} \right\rangle}{\partial x_i} + \frac{1}{V_a} \int_S \overline{f(\mathbf{x})} n_i dS(x) \qquad (2)$$

The second term of the right side is to integrate function f on the solid surface, < > means the spatial average, and ¯ means the ensemble average. This would make it necessary to have a spatial averaging of pressure and shear stress. This property of the averaging operators must be carefully considered when deriving the governing equations of the model. The quantity formed by the distribution of effective volume ratio must be divided into two components: an apparent vector component that

should not be included in the drag effect, and a component that works as actual drag due to discontinuous pressure changes in the front and back of the building.

Fig. 1 shows the sketch for the pressure balance in a control volume with an effective volume ratio distribution in the x_i direction. As shown in the figure, where the pressure is discontinuous, drag forces are at work. The pressure gradient is spatially averaged in the following.

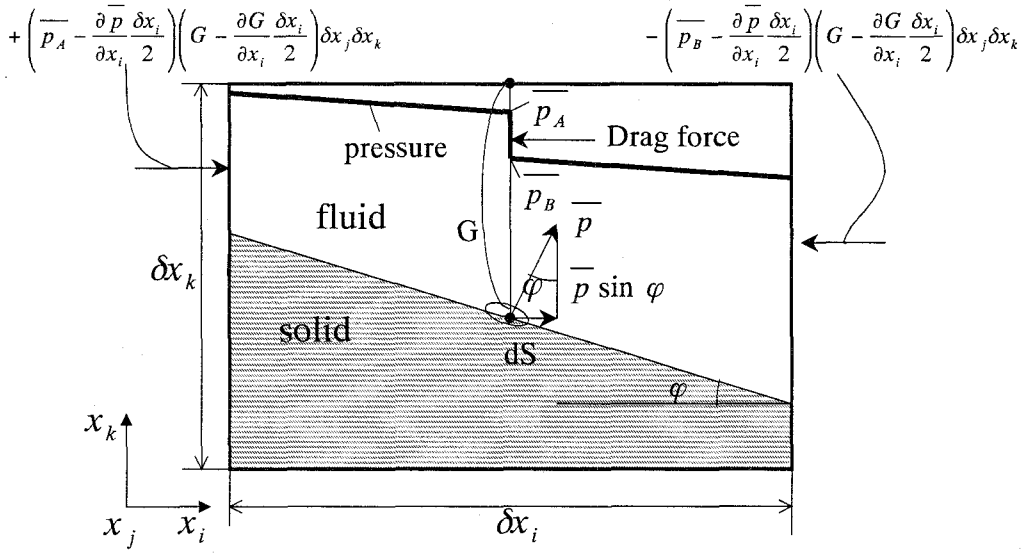

Figure 1 The pressure balance of a control volume with an effective volume ratio distribution

$$-\left\langle\frac{\partial p}{\partial x_i}\right\rangle=\left\{\left(\overline{p_A}-\frac{\partial\bar{p}}{\partial x_i}\frac{\delta x_i}{2}\right)\left(G-\frac{\partial G}{\partial x_i}\frac{\delta x_i}{2}\right)\delta x_j\delta x_k/V_a-\left(\overline{p_B}+\frac{\partial\bar{p}}{\partial x_i}\frac{\delta x_i}{2}\right)\left(G+\frac{\partial G}{\partial x_i}\frac{\delta x_i}{2}\right)\delta x_j\delta x_k/V_a\right.$$

$$\left.+\frac{1}{V_a}\int\overline{p}n_i dS\right\}\Big|_{(\delta x_i,\delta x_j,\delta x_k\to 0)}=-\frac{\partial\langle\bar{p}\rangle}{\partial x_i}-\left(\overline{p_B}-\overline{p_A}\right)/\delta x_i \qquad (3)$$

where p is pressure, x is distance, and S is the surface area. The drag force exerted by buildings on the airflow is caused by the pressure discontinuity and the frictional force at the solid surface. Equation 4 shows the approximation for the drag force (Wilson, 1988). The first term of the left-hand side of this equation is the pressure, while the second term is the frictional force at the solid surface.

$$\left(\overline{p_B}-\overline{p_A}\right)/\delta x_i+\frac{1}{V_a}\int_S\overline{\tau_{ik}}n_k dS=aC_{fl}\overline{u_i}\left(\langle\overline{u_k}\rangle^2\right)^{1/2} \qquad (4)$$

where C_{fl} is the drag coefficient, and a signifies the area density, defined as the projected solid surface area within an unit volume in x_i direction. In this study, the drag coefficient C_{fl} is 0.875 for building (Maruyama, 1989), and 0.2 for forest (Yamada, 1982).

2) Effect of thermal stratification

Thermal stratification effects on the transport of momentum, heat and mass in the vertical direction have been investigated by Mellor (1973), Yamada (1975), Launder (1975) and Gambo (1978). In this paper, the scheme proposed by Launder (1975) is employed to improve the standard κ - ε model. Applying IP theory (Launder *et al.*, 1975) to the rapid terms of pressure strain correlation and pressure-temperature variation gradient correlation, the Reynolds stress and thermal flux were expressed with the following equations (Launder, 1975):

$$-\overline{u_1'u_3'} = \phi \frac{k\overline{u_3^2}}{\varepsilon} \frac{\partial \langle \overline{u_i} \rangle}{\partial x_3} - \phi\beta \frac{gk\overline{u_1'\theta'}}{\varepsilon} \qquad (5)$$

$$-\overline{u_1'\theta'} = \phi_\theta \frac{k}{\varepsilon} \left(\overline{u_1'u_3'} \frac{\partial \langle \overline{\theta} \rangle}{\partial x_3} + \frac{1}{2} \overline{u_3'\theta'} \frac{\partial \langle \overline{u_1} \rangle}{\partial x_3} \right) \qquad (6)$$

$$-\overline{u_3'\theta'} = \phi_\theta \frac{k\overline{u_3^2}}{\varepsilon} \frac{\partial \langle \overline{\theta} \rangle}{\partial x_3} + 0.8\phi_\theta \beta \frac{gk^2 \overline{u_3'\theta'}}{\varepsilon^2} \frac{\partial \langle \overline{\theta_v} \rangle}{\partial x_3} \qquad (7)$$

where ϕ and ϕ_θ are constants, β is the volume expansion coefficient, and g is the gravitational acceleration. By rewriting these equations into eddy viscosity forms, we can separate horizontal and vertical parts in the coefficients of eddy viscosity and eddy thermal diffusion. In this paper, the buoyancy effect of the κ - ε model is summarized in the eddy viscosity model coefficient C_μ of the vertical direction and turbulence Plandtl number P_{rt}. These were rewritten as the function of the flux Richardson number R_f as follows.

$$C_\mu = \frac{0.8\phi\gamma - 0.5\gamma(\phi_\theta - \gamma)}{0.8\gamma + \phi(\phi_\theta - \gamma)} \frac{0.53 - 0.94R_f}{1 - R_f} \qquad (8)$$

$$P_{rt} = P_{rt0} \frac{1.59 - R_f(1.5\phi_\theta + 2.82)}{1.59 + R_f(3\phi - 5.22)} \qquad (9)$$

$$\gamma = \phi_\theta \frac{1.59 - 5.22R_f}{1.59 - 2.82R_f} \qquad (10)$$

The dependence of the coefficient C_μ and the turbulence Plandtl number P_{rt} on the flux Richardson number R_f, is shown in Fig. 2. In the figure, wind tunnel data by Webster (1964) and field data of Kondo *et al.* (1978) are also shown together with computational results by a Level 2.5 closure scheme (Yamada, 1975). It can be seen that results by the present model agree better with experimental data than those from the Level 2.5 of Yamada (1975). Thus, our closure scheme is used for the coming analysis. Table 1 is an overview of the equations of three-dimensional turbulent flow models of the urban atmospheric boundary layer. It should be noted that for a variable topography, we used a terrain following coordinate system (Yamada and Bunker, 1988).

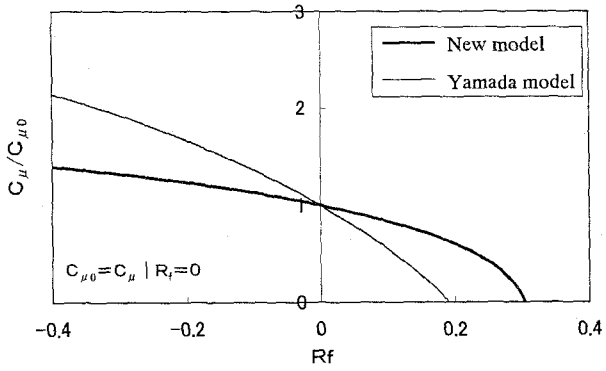

Figure 2a Eddy viscosity model coefficient C_μ

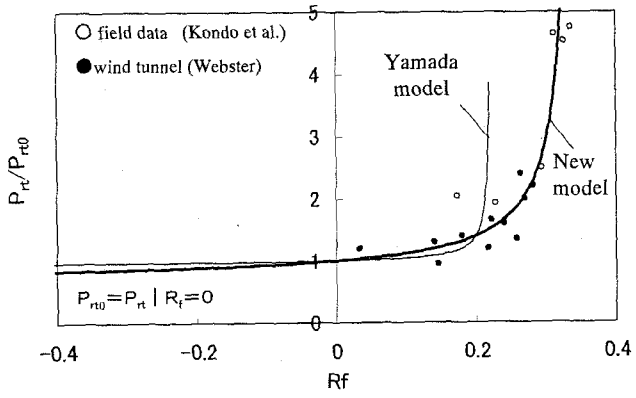

Figure 2b Turbulence Plandtl number P_{rt}

Table 1 Equations of three-dimensional turbulent flow models of urban boundary layers

eq. of continuity	$\frac{1}{G}\frac{\partial G<\overline{u}_i>}{\partial x_i}=0$
eq. of N. S.	$\frac{\partial\langle\overline{u}_i\rangle}{\partial t}+\frac{1}{G}\frac{\partial G\langle\overline{u}_i\rangle\langle\overline{u}_k\rangle}{\partial x_k}=-\frac{1}{\rho_a}\frac{\partial\langle\overline{p}\rangle}{\partial x_i}+\frac{1}{G}\frac{\partial}{\partial x_k}\left(G\nu_t\frac{\partial\langle\overline{u}_i\rangle}{\partial x_k}\right)$ $-\beta g_i\delta_{i3}\left(\langle\overline{\theta}_v\rangle-\theta_{v0}\right)-\varepsilon_{ik\lambda}\Omega_k\overline{u_\lambda}-aC_{fl}\left(\langle\overline{u_k}\rangle^2\right)^{0.5}\overline{u_i}$
eq. of heat transport	$\frac{\partial\langle\overline{\theta}\rangle}{\partial t}+\frac{1}{G}\frac{\partial G\langle\overline{u}_k\rangle\langle\overline{\theta}\rangle}{\partial x_k}=\frac{1}{G}\frac{\partial}{\partial x_k}\left(G\frac{\nu_t}{P_{rt}}\frac{\partial\langle\overline{\theta}\rangle}{\partial x_k}\right)+\frac{\langle\overline{H_a}\rangle+\langle\overline{H_s}\rangle}{GC_p\rho_a}$
eq. of vapor transport	$\frac{\partial\langle\overline{q}\rangle}{\partial t}+\frac{1}{G}\frac{\partial G\langle\overline{u}_k\rangle\langle\overline{q}\rangle}{\partial x_k}=\frac{1}{G}\frac{\partial}{\partial x_k}\left(G\frac{\nu_t}{P_{rt}}\frac{\partial\langle\overline{q}\rangle}{\partial x_k}\right)+\frac{\langle\overline{Q_a}\rangle+\langle\overline{Q_s}\rangle}{G\rho_a}$
k eq.	$\frac{\partial k}{\partial t}+\frac{1}{G}\frac{\partial G\langle\overline{u_k}\rangle k}{\partial x_k}=\frac{1}{G}\frac{\partial}{\partial x_k}\left(G\frac{\nu_t}{\sigma_\kappa}\frac{\partial k}{\partial x_k}\right)-\varepsilon+g_i\beta\frac{\nu_t}{P_{rt}}\frac{\partial\langle\overline{\theta_v}\rangle}{\partial x_k}\delta_{i3}$ $+\nu_t\left(\frac{\partial\langle\overline{u_i}\rangle}{\partial x_k}+\frac{\partial\langle\overline{u_k}\rangle}{\partial x_i}\right)\frac{\partial\langle\overline{u_i}\rangle}{\partial x_k}+aC_{fl}\left(\langle\overline{u_k}\rangle^2\right)^{3/2}$
ε eq.	$\frac{\partial\varepsilon}{\partial t}+\frac{1}{G}\frac{\partial G\langle\overline{u_k}\rangle\varepsilon}{\partial x_k}=\frac{1}{G}\frac{\partial}{\partial x_k}\left(G\frac{\nu_t}{\sigma_\varepsilon}\frac{\partial\varepsilon}{\partial x_k}\right)$ $+\frac{\varepsilon}{\kappa}\left(\begin{array}{l}C_{1\varepsilon}\nu_t\left(\frac{\partial\langle\overline{u_i}\rangle}{\partial x_k}+\frac{\partial\langle\overline{u_k}\rangle}{\partial x_i}\right)\frac{\partial\langle\overline{u_i}\rangle}{\partial x_k}-C_{2\varepsilon}\varepsilon\\ +C_{3\varepsilon}g_i\beta\frac{\nu_t}{P_{rt}}\frac{\partial\langle\overline{\theta_v}\rangle}{\partial x_k}\delta_{i3}+C_{p\varepsilon}\frac{k^{3/2}}{L_0}\end{array}\right)$
Symbols	t: time, x: distance, u: wind speed, θ: potential temperature, θ_v: virtual potential temperature, q: mixing ratio, p: pressure, k: turbulent energy, ε: viscosity dispersion rate, ρ_a: density of air, c_p: specific heat, H_a: heat release quantity in atmosphere, H_s: heat release quantity at surface Q_a: moisture release quantity in atmosphere, Q_s: moisture release quantity at surface G: effective volume ratio, a: drag area, C_{fi}: Drag coefficient, P_{rt}: turbulent Plandtl number ν_t: coefficient of eddy viscosity, g_i: external force acceleration(g_3=-9.80665m/s²), β: volumetric expansion rate, $\varepsilon_{ik\iota}$: alternation tensor, Ω_k: Coriolis parameter
Constant	σ_k=1.0, σ_ε=1.3, $C_{1\varepsilon}$=1.49, $C_{2\varepsilon}$=1.92, $C_{3\varepsilon}=C_{1\varepsilon}$(unstable),$C_{3\varepsilon}$=0(stable), $C_{p\varepsilon}$=0.5

3. Building air conditioning model

The sketch of the building air conditioning model is shown in Fig. 3. The sensible and latent heat exchange between wall and roof of the building with the air is coupled into the turbulent model for the atmospheric boundary layer. With accounting for the thermal properties of the construction material of the walls and roof, the heat conduction equation inside the walls and roof is solved, and the heat exchange between the walls and roof and indoor air is evaluated. The heat flow through the windows and walls, the penetration of solar radiation through the windows, the indoor exhausted heat, and the in-out door heat exchanged through ventilation are all computed. The source term in the heat transport equation (Table 1) represents the thermal gains due to the divergence of longwave radiation, the sensible heat exchange between walls and roof with outside air, and the heat released from the air conditioning system. These are discharged into the nearest computational grids. In the radiation analysis inside the building canopy, the sunlit and shaded portion of walls and ground surface, the view factors of each surface for surrounding surfaces, and multiple reflections are all considered.

Fig. 4 shows a sketch for the computation of view factors from each surface for other surfaces. View factors are calculated using the bulk information of building ratio and building height at each mesh. Fig. 5 shows the relationship between outside air temperature, partial load of the heat pump η, and the so called Coefficient Of Performance (COP) of the heat pump, defined as the ratio between the

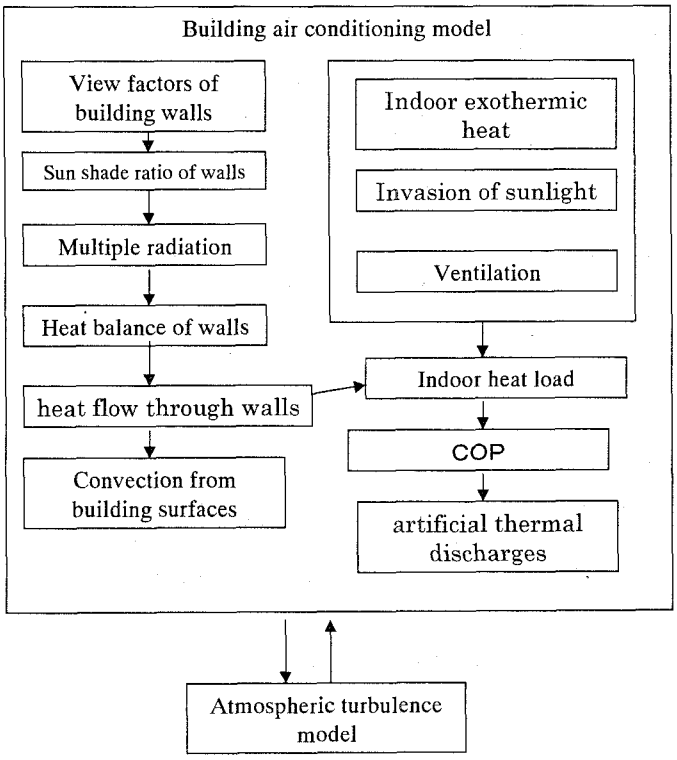

Figure 3 Building air conditioning model

indoor heat load and the required cooling electricity (Ashie *et al.*, 1999). It can be seen that the COP decrease with an increase in the outside air temperature.

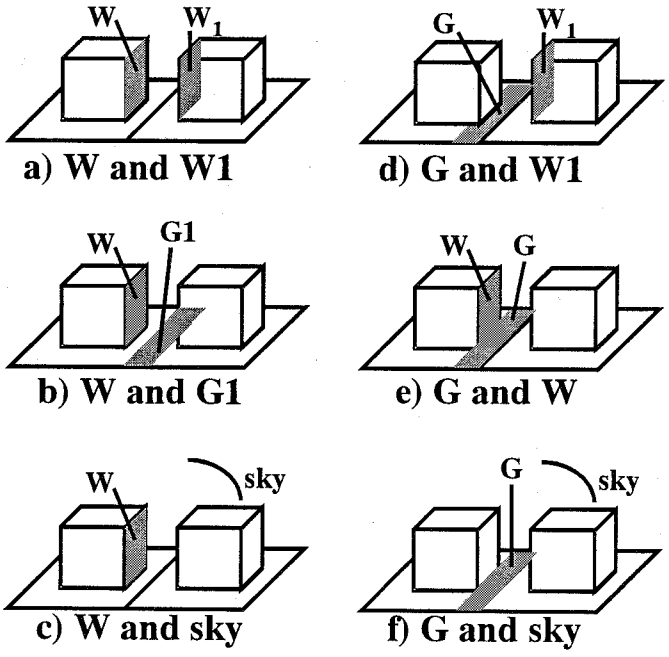

Figure 4 The view factors from each surface for other surfaces (W: building wall, G:soil surface, sky: sky)

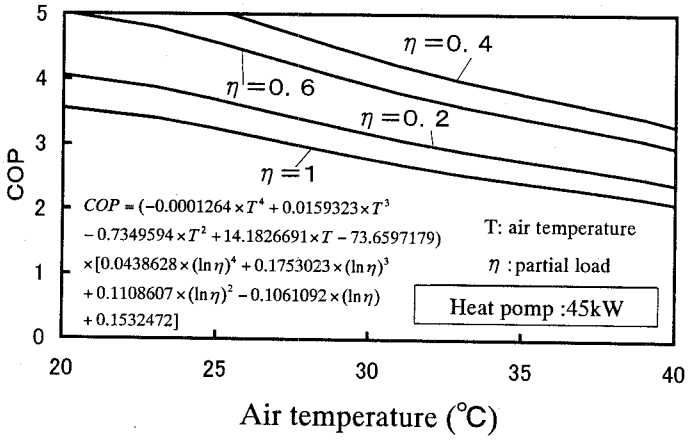

Figure 5 COP characteristics of the heating unit

4. Regional Analysis

In this section, we present results of the analysis on air flow and air temperature on a region covering the Kanto area in Japan as shown in Fig. 6. A two-nested layer input data of area 1 (480km*400km, 8km grid) and area 2 (122km*122km, 2km grid) was provided using the DEM (250m elevation grids) of the Geological Survey Institute and numerical land data (100m grids) of the National Land Agency. We used the popular roughness model for buildings, asphalt and so on in area 1 as same as Ichinose *et al.* (1999). The anthropogenic heat discharge in area 1 was ignored. The drag model was adapted for forests proposed by Yamada (1982). The feed back effect of building air conditioning system was simulated only for area 2 by the building drag model. In area 2, the building lots were referred to in the numerical land data, but this data did not include detailed information on such things as the proportion of floorspace to area of building lot. Then, averaged building-related data, which were estimated from materials from the Tokyo Metropolitan Government, were set as follows: the ratio of building area to lot area 50%, 3 stories, RC structure (for thermal characteristics). Actually, since building use differs from one region to another, it will be necessary for future analyses to include more detailed building data. The logarithm low was adopted to set the initial profile of air temperature and velocity. The initial potential temperature at ground level is 24 ℃. The boundary condition at horizontal sides was assumed to be zero gradients for air temperatures and velocities.

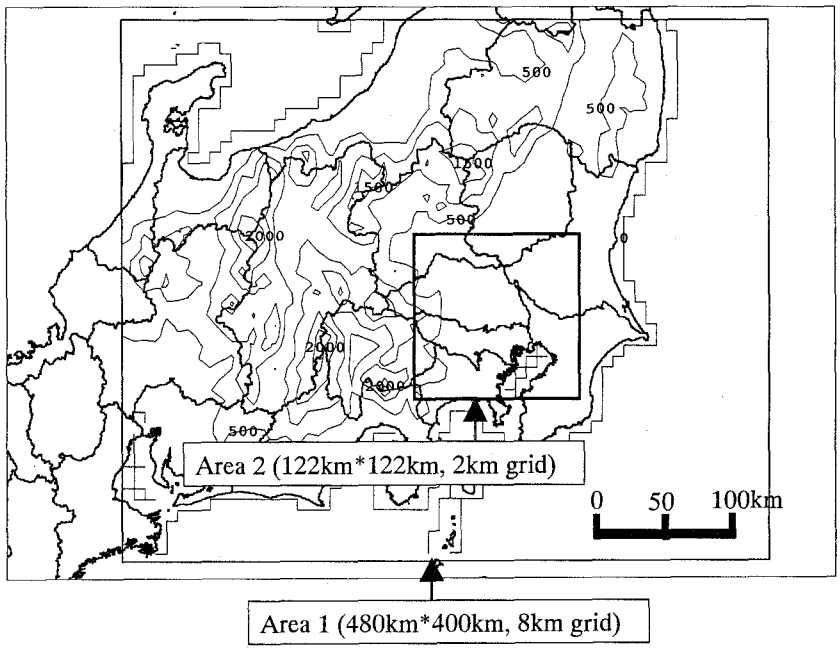

Figure 6 Analyzed area with altitude data

Fig. 7 shows the results of temperature calculations at 3 p. m. in area 1. A high-temperature region centered on the Tokyo Metropolitan Area is clearly seen. Inland areas, such as landlocked Saitama Prefecture (point B in Fig. 7), are warmer than Tokyo (point A in Fig.7), which is near the

coast. In the Boso Peninsula of Chiba Prefecture (point C in Fig. 7), the temperature is more comfortable due to sea breezes. These features agree with the measurement results of Amedas data (Ashie, 2001).

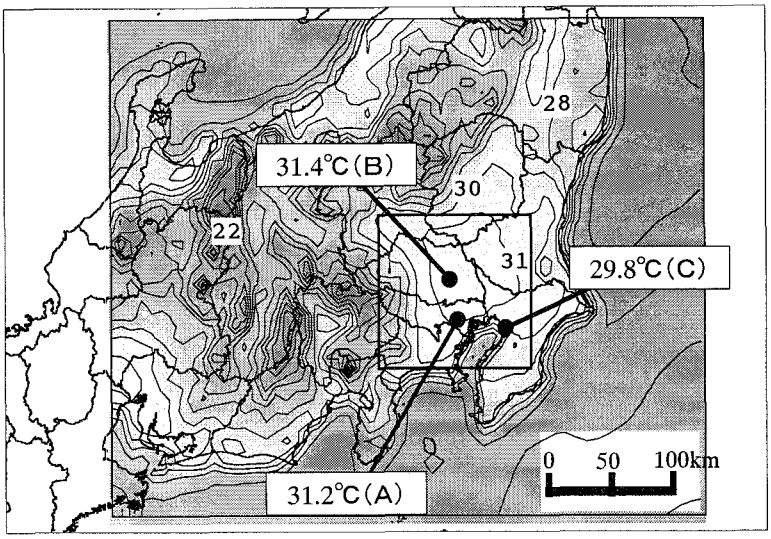

Figure 7 Summertime temperature distribution
(area 1, analytical results for 3:00 p.m.)

Fig. 8 shows the horizontal distribution of wind velocity in area 1 at the same time as that in Fig. 7. The sea breezes can be clearly seen in Fig.8. The measurement data using Amedas data is shown in Fig. 9. An available weather condition on sunny day with weak velocity was selected for a comparison with the data of numerical simulation. Compareing the wind pattern shown in Fig.8 and Fig.9, it can be remarked that there is good agreement between computed results and observational data. In particular, the SE sea breezes originating off the Kashima coast and the southerly breezes from Sagami Bay converging at the West of Saitama Prefecture are well simulated. Fig. 10 shows the distribution of artificial heat discharge in area 2, in terms of the energy consumption of air conditioners and the total air conditioning load per unit area. The peak of the air conditioning artificial heat discharge of about 100-150 W/m^2, is observed in the center of the Tokyo Metropolitan Area, which clearly accounts for the lion's share of energy consumption.

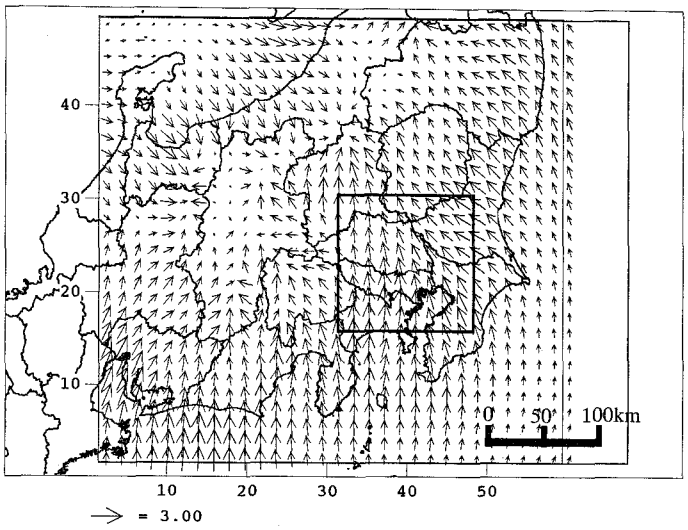

Figure 8 Summertime wind distribution in area 1
(results of analysis for 3:00 p.m.)

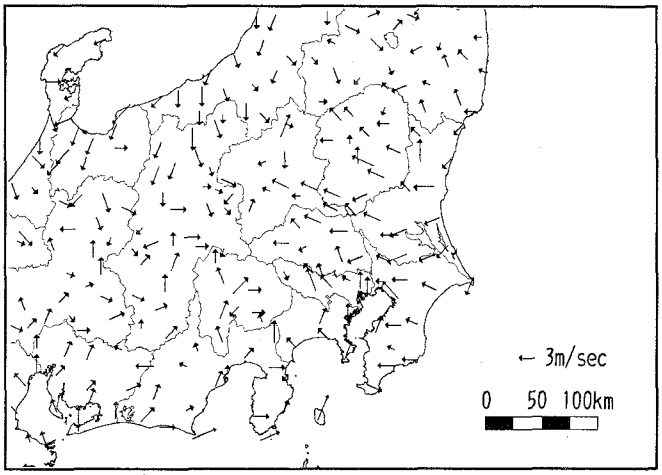

Figure 9 Wind distribution according to AMeDAS
(at 3:00 p.m. on 21 Aug 1997)

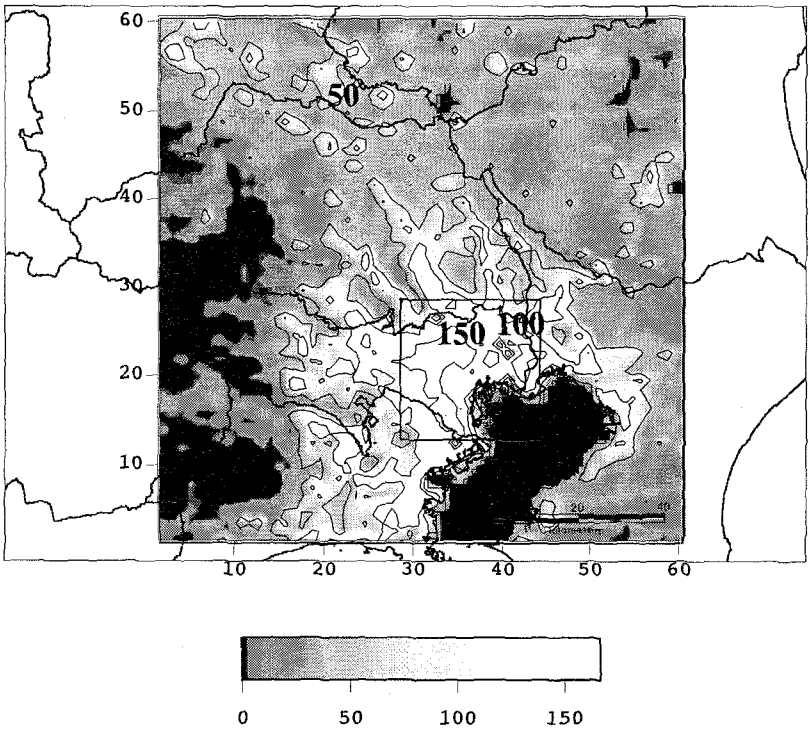

Figure 10 Distribution of artificial heat release from buildings in area 2 (W/m^2 at 3:00 p.m., as per the analysis)

5. Local-scale analysis

This section deals with results of the simulation over a local scale area. A 500m-square area shown in Fig. 11 was derived using GIS data for land-use in Tokyo. Building ratio, number of stories, structure, green area, roads, etc. were converted into 10m polygonal grid units as the input data of the analysis program. This analysis assumed home air conditioners were dominant in houses and multi commercial air conditioning systems were dominant in the office buildings. The area of the analysis extended up to 1500m into the air to account for the convection mixture in daytime. The atmosphere was divided into 43 meshes. Because the effect of local winds was taken into consideration, a nudging method was used to determine the daily changes in wind direction and wind speed at heights of 100-800meters. The nudging parameter was assumed to be five times as much as the Coriolis parameter (Yamada, 1989).

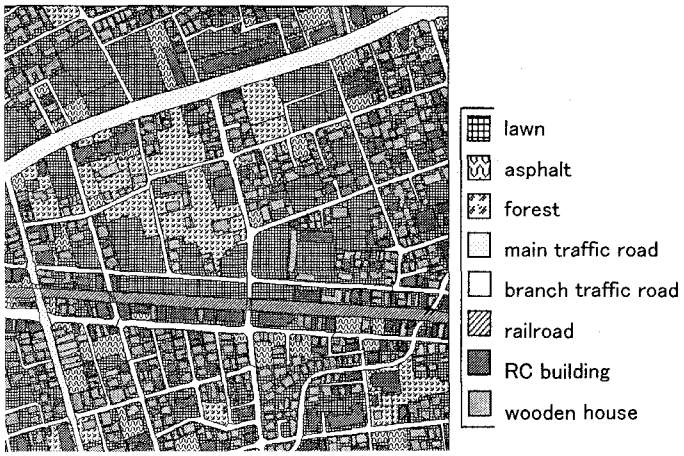

Figure 11 Land-use distribution in an analyzed district of Tokyo (based on GIS data)

Fig. 12 shows the computed temperature distribution. It can be observed in the figure that cool spots were formed in green areas with air temperatures of about 0.5-1.0℃ lower than that in the surrounding areas.

From Fig. 13, we can get a good idea of the tremendous influence of land cover on temperature distribution at ground level. It is very clear that streets were much warmer than other areas, while areas planted with trees were the coolest. Sometimes the temperature difference between these two extremes was 20℃ or more.

Fig. 14 shows the relation between the 10m grid temperatures and the COP of residential and office areas for the same time of day. In both areas, as temperature increased COP values tended to decrease, by about 9% for every 1℃ drop in temperature.

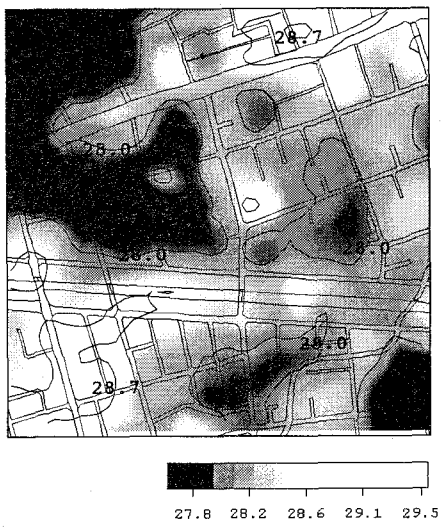

Figure 12 Temperature distribution obtained from analytical results (3:00 p.m. in summer)

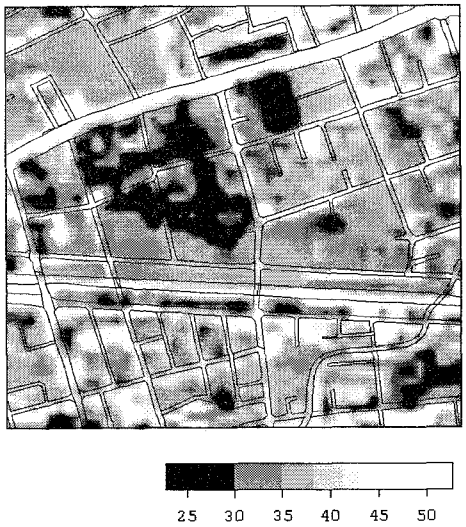

Figure 13 Surface temperature distribution obtained from analytical results (3:00 p.m. in summer)

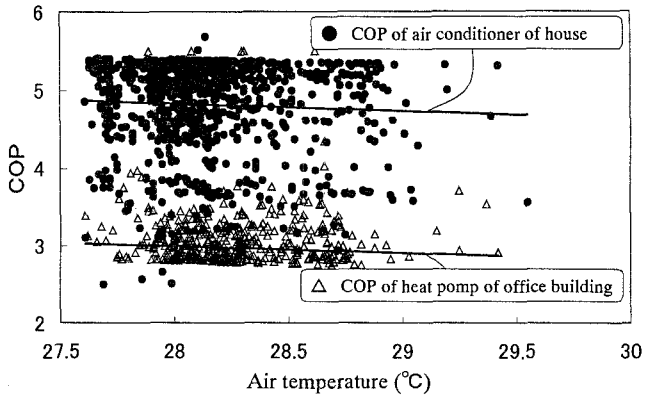

Figure 14 Relation between air temperature and COP

6. Investigation of energy-saving effects of green areas

In the aforementioned district, there is a substantial proportion of green areas (9% trees, 39% grass), but it is predicted that future development will result in at least some of this area being paved over for parking lots and high-rise buildings. Therefore, we made simple calculations of what would happen if all the greenery were covered by asphalt in order to examine its effects on temperature and

energy load. Figure 15 shows a comparison of the estimated thermal environment after development with the calculations for the current state. The nighttime value is the average for 5:00 a.m. in the district, while the daytime temperature is the average value for 3:00 p.m. "District energy" refers to the total daily amount of energy consumed in the district for air conditioning. The energy for cooling was derived from indoor load and COP values.

Development of the area would result in an increase in both daytime and nighttime temperature of about 0.5-0.6℃, which would be expected to have some effect on the heat index during the waking and sleeping hours of the day. Energy consumed by air conditioning would rise by about 8%, adding about 7.6 million yen to the district electric bill during the season.

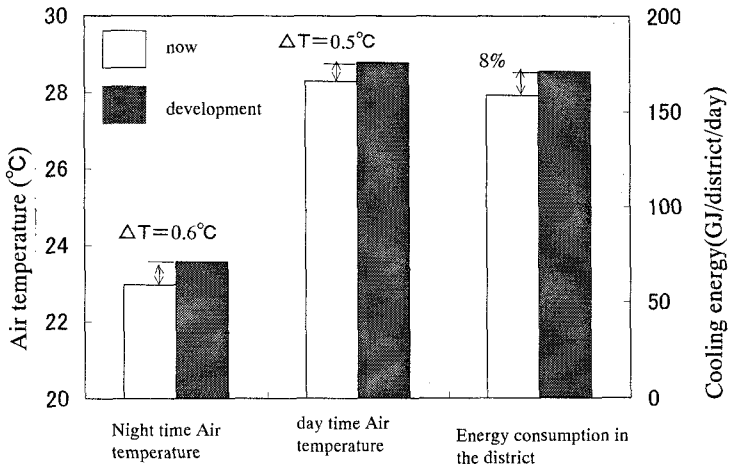

Figure 15 Estimated effects of thermal environment of developed area, based on numerical calculations

7. Conclusions

An attempt was made to estimate an urban thermal environment at the regional and local scales. As a result, it was found that residents of areas covered with about 50% vegetation had passive energy savings of about 8% due to the effects of the greenery. This analytical method can be applied to various scales of urban development. We hope that it will be used in quantitative investigations for policies aimed at reducing the heat island effect.

Acknowledgements

We would like to thank the Heat Island Analytical Investigation Committee supported by the Office of Sensory Pollution and Air Quality, Ministry of Environment for allowing us to use their data for the regional analysis.

References

Ashie, Y., S. Tanaka and T. Yamamoto (1999) : Heat discharge characteristics of air conditioning systems of office buildings, Transactions of the SHASE of Japan, No.75, pp.89-97 (in Japanese)

Ashie, Y. (2000): chapter 6 Metropolis Tokyo exposed to the land and sea breezes, Klimaatlas of urban environment (ISBN4-324-06278-1), AIJ, gyosei (in Japanese)

Ashie, Y. (2001): investigation and analysis of heat island, Midori no dokuhon 57, kohgai taisaku gijyutu dohkohkai, pp.9-14 (in Japanese)

Craspite, G. H., E. Rotstein and S. Whitaker (1986): A general closure scheme for the method of volume averaging, Chemical engineering Science, 41-2, pp.227-235

Gambo, K.(1978): Notes on the turbulence closure model for atmospheric boundary layer, J. Meteorol. Soc. Japan, 56-5, pp.466-480

Head office of Japanese government for the promotion on the ameliorating global warming (1997): board outline for the promotion on the ameliorating global warming (in Japanese)

Ichinose, T., K. Shimodozono and K. Hanaki (1999): Impact of anthropogenic heat on urban climate in Tokyo, Atmos. Enviromment 33, pp.3897-3909

Japan electric association: The situation of electric business, 1991 (in Japanese)

Kimura, F. and S. Arakawa (1983): A numerical experiment in the nocturnal low level jet over the Kanto plain, J. Meteorol. Soc. Japan, 61-6, pp.848-861

Kitada, T, K. Okamura, and S. Tanaka (1998): Effects of topography and urbanization on local winds and thermal environment in the Nohbi plain, coastal region of central Japan - A numerical analysis by mesoscale meteorological model with k-e turbulence model, J. Appl. Meteorol. Vol.37, No.10, pp.1026-1046

Kondo, J., O. Kanechika and N. Yasuda (1978): Heat and momentum transfers under strong stability in the atmospheric surface layer, J. Atmos. Sci., 35, pp. 1012-1021

Launder, B. E.(1975): On the effects of a gravitational field on the turbulent transport of heat and momentum, J. Fluid Mech., 67,pp.569-581

Launder, B. E., G. J. Reece and W. Rodi (1975):Progress in the development of Reynolds stress turbulence closure, J. Fluid Mech., 68, pp.537-566

Maruyama, K. (1989): Numerical calculation of turbulent boundary layer using refined k- ε model in consideration of drag and volume change of roughness elements, J. Struct. Constr. Eng., AIJ, No.404, pp.75-81 (in Japanese)

Mellor, G. L. (1973): Analytic prediction of the properties of stratified planetary surface layers, J. Atmos. Sci., 30, pp.1061-1069

Mitsubishi Research Institute (2000): primary sources of the committee on the research of urban heat island organized by Ministry of Construction (in Japanese)

Murakami, S., S. Kato and T. Chikamoto, D. Laurence and D. Blay (1996): New low-Reynolds-number k- ε model including damping effect due to buoyancy in a stratified flow field, Int. J. Heat Mass Transfer, 39, 16, pp. 3483-3496

Murakami, S., A. Mochida, S. Kim, R. Ooka (1997): Influence of land-use conditions on velocity and temperature fields over Kanto plane (Mathematical models for urban climate based on turbulence model proposed by Mellor-Yamada), J. Archit. Plann. Environ. Eng., AIJ, No.491, pp.31-39 (in Japanese)

Yamada (1975), T.: The critical Richardson number and the ratio of the eddy transport coefficients obtained from a turbulence closure model, J. Atmos. Sci., 32, pp.926-933

Yamada, T. (1982): A numerical model study of turbulent airflow in and above forest canopy, J. Metorol. Soc. Japan, Vol. 60-1, pp. 439-454

Yamada, T. and S. Bunker (1988): Development of a nested grid, second-moment turbulence closure model and application to the 1982 ASCOT brush creek simulation, J. Appl. Meteorol., 27, pp.562-578

Yamada, T. and S. Bunker (1989): A numerical model study of nocturnal drainage flows with strong wind and temperature gradients, J. Appl. Meteorol., 28, pp. 545-554

Webster, C. A. G. (1964): An experimental study of turbulence in a density stratified shear flow, J. Fluid Mech., 19, pp. 221-245

Wilson, J. D. (1988): A second-order closure model for flow through vegetation, Bounday-Layer Meteorol., 42, pp. 371-392